This is a repository copy of *28GHz rural close-to-ground propagation field test results and models*.

White Rose Research Online URL for this paper:
https://eprints.whiterose.ac.uk/211842/

Version: Published Version

eprints@whiterose.ac.uk
https://eprints.whiterose.ac.uk/

IEEE Open Journal of
Antennas and Propagation

28GHz Rural Close-to-Ground Propagation Field Test Results and Models

SUMIN DAVID JOSEPH[1](Member, IEEE), BILL GAVIN[1], AND EDWARD A BALL[1] (Member, IEEE)
[1]The University of Sheffield, Sheffield, UK

CORRESPONDING AUTHOR: Sumin David Joseph (e-mail: s.d.joseph@sheffield.ac.uk).

ABSTRACT A set of 28 GHz close-to-ground propagation measurements are conducted for different rural outdoor scenarios at the National Spectrum Centre, Aberystwyth. A bespoke correlation based channel sounder and horn antennas are employed in the measurement system. The measurements provide large-scale path loss, time domain impulses and channel measurements that will be beneficial for rural future millimeter wave communication systems. Different scenarios, such as straight and elevated paths, zig-zag curved road and curved road in woods are explored and log-normal models are extracted. Propagation measurements in diverse terrains including hill, grass land, dense forest and buildings are also conducted. The path loss predictions of existing foliage loss models like Weissberger , ITU-R, COST and FITU-R are investigated with frequency and distance. Then, the measured path losses are compared with these models. Predicted pathloss values of these models are overestimated at 28 GHz in dense tree forest after 50 m. Strong reflections are observed in the propagation through buildings at log(d) distance of 1.6 and 1.9. Similar path loss attenuations and fixed offset values (nearly 22 dB more than free space) are observed in the propagation through the dense forest and curved road in woods. The presented close-to-ground propagation research is significant for future military applications and mobile device-to-device communications.

INDEX TERMS device-to-device, foliage, path loss, propagation, millimeter-wave systems.

I. INTRODUCTION

Innovations in wireless technologies encourage an explosion in wireless data traffic due to the advancement in development of electronic devices that can deliver, monitor, transfer, and record billions of terabytes of data every year [1]-[3]. The sudden rise in wireless technologies and applications has created the concern of limited spectrum resources below 6 GHz [4]-[6]. Therefore, with the advent of 5G and 6G, millimeter-wave frequency bands which offer wide bandwidth and high data rates has been attracting significant attention [7]. Although certain bands are affected by water vapor and oxygen absorption, such as 57–64 and 164–200 GHz bands, millimeter-wave communications can offer 10's of Gb/s of data over the whole spectrum. However, it is commonly believed that due to factors such as high propagation loss and susceptibility to blockage, millimeter-wave bands are not practicable for mobile communications. But the introduction of mm-wave 5G New Radio (NR) has transformed that misconception [8]. As these frequency bands have a short wavelength, high gain arrays or MIMO systems are quite necessary for millimeter-wave communications. Short wavelength is advantageous to accommodate array or massive MIMO implementations and it can significantly improve wireless access and throughput performance [9]. Propagation loss in the millimeter-wave bands is relatively high compared to microwave bands, due to blocking effects when not line of sight (LOS). Consequently, the utilization of beamforming and beam tracking features in phased arrays becomes crucial in 5G networks, both at the base station and user ends, to establish highly directional transmission links and counteract propagation losses [10]. Similarly, building penetration losses are considerably higher in millimeter-wave bands, posing challenges in passing through building walls and leading to significant degradation in data rate, spectral efficiency, and energy efficiency. As a result, 5G networks are adopting 28 GHz millimeter-wave systems for outdoor spaces. Considering all these factors, channel propagation characteristics in millimeter-wave bands differ significantly from those below 3 GHz, rendering most existing channel characteristics measurements and models irrelevant to the millimeter-wave bands [11]. Hence, fundamental knowledge of millimeter-wave channel propagation characteristics , including accurate and reliable channel models, is critical for developing 5G wireless communication systems.   .

Vegetation and foliage are one of the critical factors in many of the real life outdoor applications. Moreover, the vegetation attenuation and absorption in the millimeter-wave bands are much more prominent than in the sub 6GHz conventional bands [12]. Several researchers have investigated and analyzed the propagation measurements and channel models in various scenarios using channel sounders [13],[14]. In [15], an explanation based on radiative energy transfer theory was presented to analyze the attenuation caused by vegetation. A numerical algorithm to calculate the foliage attenuation for millimeter-wave bands based on the radiative transfer equation was introduced in [16]. Scattering by tree branches has been evaluated using ray-based model and incorporated with a ray tracing tool in [17]. A 2D ray tracing model for micro and millimeter-wave propagation through vegetation was presented in [18] and analyzed with discretized radiative energy transfer approach. Nevertheless, the influence of vegetation can also be analyzed through experimental approaches. An experimental and theoretical study of wave propagation in woods was conducted in [19]. The experiments were conducted at 9.6, 28.8, and 57.6 GHz frequency bands and in both summer and winter conditions with CW signals. An inclined 24 GHz measurements were carried out through vegetation in [20]. The transmitter antenna was placed above average tree height and receiver antenna placed near to ground. Channel measurements at 28 GHz were conducted in [21] through trees with long foliage depth and shows that additional loss in vegetated areas is linked with a saturating tendency with upper-bounded attenuation at 28 GHz. In [22], measurements were conducted in vegetated areas of residential areas. The study revealed that the tree clutter causes the strongest cluster, while the building walls form the second valid cluster in a typical residential environment.

Close-to-ground propagation holds considerable importance in scientific and military scenarios, particularly in the context of communication networks deployed in battlefield environments [24]. Substantial efforts have been dedicated to understanding the close to ground propagation of radio signals within forested environments [23]-[29]. In [23], near-ground channel measurements over a forested path at 300 and 1900 MHz is presented and compared with foliage models. Path loss in a typical plantation is investigated in [24] at VHF and UHF bands with an antenna height of 2.5 m. Foliage attenuation in a coniferous and deciduous forest is evaluated in [26],[28] and [29]. Propagation through bushes and light tree cover is analyzed in [25] and [27]. In these close-to-ground measurements, antenna heights of 1.5 and 2.1 m are utilized in [25] and [27] respectively. Nevertheless, in these close to ground reported works, the examination of foliage attenuation is limited to UHF and VHF frequency bands only. Thus, this paper is driven by the lack of research conducted in rural outdoor at near ground levels in millimeter-wave frequencies.

Most of the researchers used vector network analyzers for propagation measurements. An industrial IoT scenario

measurement at 3–4 and 38–40 GHz were conducted in [30]. A programmable VNA and necessary auxiliary equipment were used to perform measurements to 15 m. But the capabilities of VNA based measurement were restricted by the cable requirements. Fiber optic links was implemented in [31] to overcome the limitation in measurable distance. Therefore, portable equipment for channel measurements is in great demand. Some researchers are employing commercial software defined radio (SDR) for portable channel measurements. In [32], 2.2 GHz indoor measurement with 100 MHz bandwidth and 10 ns delay resolution is carried out by implementing multiple overlapping tones in a USRP. Commercial millimeter-wave boards and equipment are utilized in [33] to perform several indoor measurements at 28 GHz. Delay spread and indoor propagation loss results were presented. Detailed outdoor measurements at 28 GHz were performed in [34] and [35] with lab equipment powered from mains. In [36], 28 GHz urban microcellular channel measurement was presented with a measurement sensitivity of 170 dB. The receiver was placed on a trolley while the transmitter was mounted on a vehicle. Room reflections in line of sight was evaluated in [37] using a steerable transmitter horn and omnidirectional receiver. Most of the reported works need a PC computer to do the data control and postprocessing. Several existing systems utilize trolleys with mains-powered equipment [33]-[35], significantly restricting mobility and hindering suitability for outdoor applications in intricate environments. The transportation of expensive laboratory equipment to field test sites during adverse weather conditions would pose risks and logistical inconveniences.

Even though the millimeter-wave frequency bands like 28 GHz are vital for technologies like 5G and 6G, there are insufficient studies evaluating the pathloss in scenarios close to ground. Most of the research has focused on cellular applications with a high base station. Therefore, this paper is primarily motivated by the absence of close to ground millimeter-wave experimental studies that focus on rural outdoor scenarios. To the best of author's knowledge, this proposed work is the first investigation into millimeter-wave close to ground propagation in rural outdoor environments. However, in [39] as the work mainly dealt with testing of the developed sounder, more realistic scenarios with extensive measurements from different terrains are investigated in this work. The study extracted large-scale path loss, time domain impulses, and channel responses from measured data, and presenting log-normal models for various terrains. The path loss observed in the experiments is then compared with the path loss predicted by empirical models. The paper is organized as follows. Section II presents the basic path loss and foliage loss models. Section III describes the measurement setup and scenarios. Section IV presents the different measurement scenarios and the results of close to ground measurements. Analysis of the measurements and the findings are discussed in Section V. Finally, the conclusions are drawn in Section VI.

II. MEASUREMENT MODELS

Various categories of large-scale path loss models, including deterministic, empirical, and stochastic models, are available. However, measurement-based path loss models offer a better practical understanding of how wireless channels propagate.

A. BASIC PATH-LOSS MODELS

Path loss refers to the attenuation in electric field intensity following the transmission of an electromagnetic signal over a specific distance. In free space path loss (FSPL) model, the pathloss is mainly dependent on distance and frequency and it has the basic assumption of no hindrances or obstacles between the transmitter and receiver.

$$PL_{(FSPL)} = 20log_{10}\left(\frac{4\pi d}{\lambda}\right) dB \qquad (1)$$

where λ is the wavelength and d is the distance between transmitter and receiver [40]. In real-world terrestrial communication systems, true free-space propagation is rarely encountered. Therefore, the two-ray (plane earth) model which represents both the direct path, and the ground reflected waves can be considered as (2)

$$PL_{(2ray)} = 40log_{10}(d) - 20log_{10}(h_t h_r) dB \qquad (2)$$

where h_t and h_r denote the height of the transmit (Tx) and receive (Rx) antenna [41].

Path loss in millimeter-wave propagation can be severely affected by the obstructions in the path and reflections. Random changes in path loss can also occurs due to clutter and scattering from other objects. Therefore, in this study, the received data is fitted to a standard log-normal path loss model of form shown in (3) as in [39]

$$PL_{(d)} = nlog_{10}(d) + PL_{(offset)} + X_{\sigma} \qquad (3)$$

where n is the distance log-scaling term, $PL_{(offset)}$ the fixed offset and X_{σ} shows the ambiguity caused by shadow fading and a zero-mean log-normally distributed random variable with σ standard deviation in dB. The overall path loss can be represented as the sum of the Free-Space Path Loss (FSPL) and an additional loss commonly referred to as excess loss, excess path loss, or excess propagation loss.

B. FOLIAGE LOSS MODELS

Exponential decay (EXD) models are empirical models for predicting the increase in loss due to propagation through trees [43]. A modified exponential decay (MED) model is presented in [44] as a better prediction. The MED model is predicted to be suitable for situations where the path of the radio wave is obstructed by thick, dry, leafy trees typically found in forests at temperate latitudes.

$$PL_{(MED)} = Xf^Y d^Z dB \qquad (4)$$

where X, Y, and Z represent the values for amplitude,

frequency, and distance dependence, respectively. Here, f stands for frequency, and d signifies the depth within the vegetation. The EXD model of Lagrone to forecast the rise in loss caused by propagation through trees is as in (5) [43].

$$PL_{(Lag)} = 0.26f^{0.77}d^1 dB \qquad (5)$$

Based on the measurements from 230 MHz to 95 GHz and with a vegetation depth upto 400m, the Weissberger prediction of MED model is expressed as

$$PL_{(weis)} = 1.33f^{0.284}d^{0.588} dB, 14 < d < 400 \qquad (6)$$

$$PL_{(weis)} = 0.45f^{0.284}d^1 dB, \qquad 0 < d < 14 \qquad (7)$$

The Weissberger MED model has been shown to be suitable for scenarios where the path of the ray is obstructed by thick, dry, leafy trees commonly found in temperate-zone forests compared to EXD model [44]. Besides, the model does not consider the influence of tree characteristics, such as structure, density, or type, nor does it account for the moisture levels in leaves and branches, or wave polarization. ITU-R 235 focused on the technical guidelines and standards for the use of radio frequencies and radiocommunication systems and in the form as shown in (8)[45].

$$PL_{(Lag)} = 0.2f^{0.3}d^{0.6} dB \qquad (8)$$

The ITU-R 235-6 model, which was previously known as CCIR, has been refined based on data collected from measurement campaigns spanning the frequency range of 200 MHz to 95 GHz. The model COST 235 [46], developed using measurements conducted within the millimeter-wave frequencies range (9.6–57.6 GHz) within a cluster of trees,

$$PL_{(Lcost)} = 26.6f^{-0.2}d^{0.5} dB \qquad out\ of\ leaf \qquad (9)$$

$$PL_{(Lcost)} = 15.6f^{-0.009}d^{0.26} dB \qquad in\ leaf \qquad (10)$$

The COST 235 model is suitable for frequencies ranging from 200 MHz to 95 GHz and measurements were conducted during both seasons: when the trees have leaves and when they don't. In the study conducted by Al-Nuaimi and Stephens [47], an optimization was carried out for the three numerical parameters through a least-squares error fit using multiple sets of measurement data. These data sets were obtained under two foliage conditions, namely with leaves and without leaves, at frequencies of 11.2 and 20 GHz. Subsequently, they developed the fitted ITU-R model [47].

$$PL_{(FITUR)} = 0.37f^{0.18}d^{0.59} dB \qquad out\ of\ leaf \qquad (11)$$

$$PL_{(FITUR)} = 0.39f^{0.39}d^{0.25} dB \qquad in\ leaf \qquad (12)$$

Most of these empirically validated models rely on measured data spanning from VHF to millimeter-waves and encompasses an average foliage depth of 400 m.
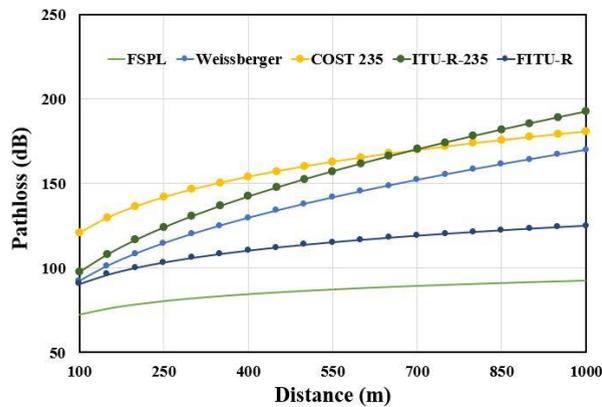
FIGURE 1. Comparison of the foliage path loss models at 1 GHz with distance

FIGURE 2. Comparison of the foliage path loss models with frequency at a fixed foliage depth of 300 m

Comparison of the different path loss models at 1 GHz with distance is presented in Fig. 1. It is clear that the excess path-loss at 100 m due to the foliage attenuation is minimum for FITU-R (18 dB) and maximum for COST235 (49 dB) model. However, the ITU-R-235 predicts maximum excess loss of 100 dB at 1000 m. Fig. 2 shows the comparison of path loss models with frequency at a fixed foliage depth d of 300 m. It can be observed that the path loss increases more steadily with frequency in Weissberger, ITU-R-235, FITU-R loss models compared to COST235. The COST235 model predicts a slight increase in path loss 165 to 183 dB while frequency changed from 10 to 90 GHz, whereas the path loss increased from 200 to 308 dB in the ITU-R-235 model. Thus, a large deviation can be observed in the predicated path loss models especially in millimeter-wave frequencies. Along with the attenuation due to foliage, it is necessary to study the pathlosses These observations inspire us to conduct additional research and measurements to determine the suitability of applying the empirical models for close to ground rural scenarios in millimeter-wave frequency bands.

III. MEASUREMENT CAMPAIGN
A. MEASUREMENT SYSTEM
The block diagram of the developed channel sounder system at 28 GHz is shown in Fig. 3. It mainly consists of a RF PCB with transmit and receive sections, a commercial software defined radio and a horn antenna [38]. In receive mode, the received signals are routed through an LNA and mixer by a SPDT switch. The mixer down converts the signal to a software controllable 2 GHz IF and routed out to SDR. Similarly, on the transmitter side the IF signals from SDR are upconverted to 28 GHz. Then the signal is amplified by a power amplifier and routed out through the SPDT switch. A PROTrinket is used in the transceiver for transmit/receive selection, hardware control and PLL frequency control. The developed system is able to report delay spread and path loss. By adjusting the ADF4372 (local oscillator)) and low pass filters, it is possible vary the IF frequency from 2GHz [39], if required. Horn antennas with a gain of 20 dBi and 17^0 beam width are utilized in the Tx/Rx chains. High gain directional antenna can compensate for the high path loss to enable a reasona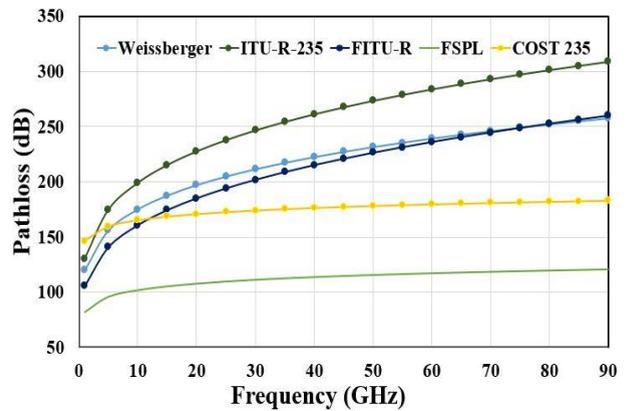ble link budget, rather than an omnidirectional low gain monopole antenna in millimeter-wave measurements. The Tx and Rx antennas are placed in LoS initially and manually aligned to each other to maximize the received signal strength. We employed lasers to confirm alignment of the Tx and Rx. Our work is therefore mainly analysing the propagation in direct LoS conditions. Most of the outdoor scenarios in this work don't have any sources of reflections away from the LoS. Only the last described scenario (with the farm buildings), deliberately excites non LoS paths and has some reflections - our test was properly constructed to receive them with the available beamwidth.

B. MEASUREMENT ALGORITHM
The 28 GHz propagation measurements were performed using pseudo random binary sequences modulated into BPSK as the transmitted signal. In the receiver side, the known transmitted signal and the received IQ data are correlated as in [39] to obtain the channel response as in (13).

$$C = IFFT[R(f) * T(f))] \qquad (13)$$

$R(f)$ and $T(f)$ are the FFTs of receive time sample series $r(n)$ and known transmit sequence $t(n)$. C can be considered as the channel impulse response in time domain. Thus, it is possible to evaluate the RF power and received delay spread. Amplitude equalization is needed to implement for the recovered Rx signal to eliminate the effects of the sinc shape of the BPSK signal and the SDR filters in the receive chain using (14), for FFT spectrum bin s out of N.

$$Response[s] = \left| sinc(\frac{s}{N}) \right|^P \qquad (14)$$

Exponent p denotes the hardware imperfections, and it can be determined by laboratory characterization. The receiver works in two gain modes for achieving best dynamic range: high and low gain mode. For long range measurements, high gain mode $R_{Gain} = 50$ is suitable between -110 to -45 dBm. Low gain mode $R_{Gain} = 20$ is preferred for short range measurements. To obtain the actual received signal strength, a frequency dependent correction factor based on the RF gain and cable losses need to be considered. So, using the resolved impulse magnitude x from C in (13), the actual received signal strength can be estimated as
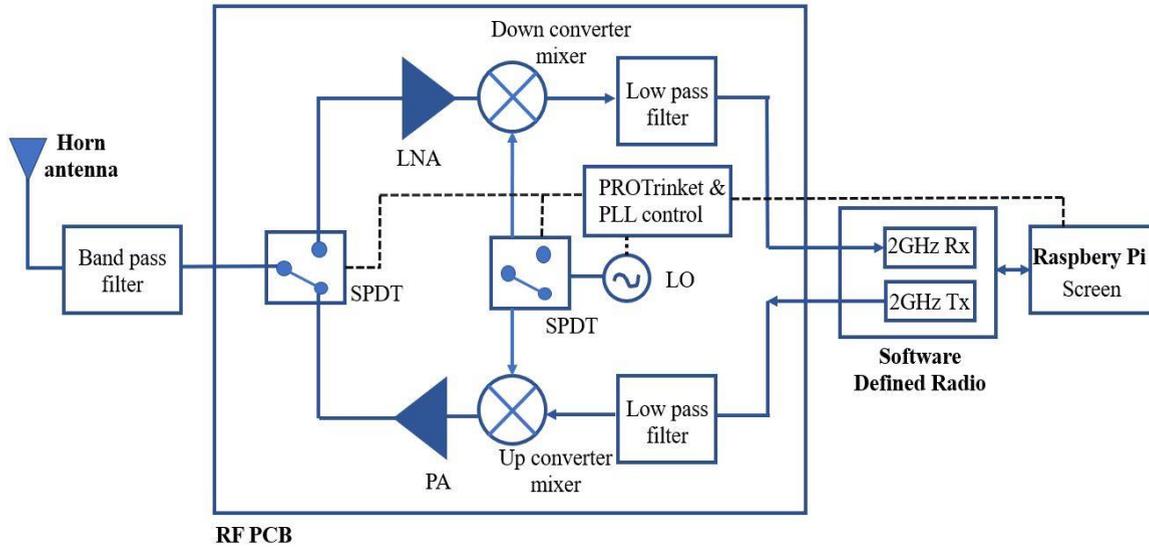
FIGURE 3. Block diagram of the channel sounder.

$$Signal\ strength\ = R_{scale}20log_{10}(x) + R_{correction} \quad (15)$$

$R_{scale} \approx 1$ and $R_{correction}$ is -180 and -200 for $R_{Gain} = 20$ &50 respectively. These values are found using initial lab calibration. A calibrated lab RF signal generator is used to generate the PRBS modulated sounder signal for calibration. No external synchronization is needed in this sounder to measure the channel frequency response and delay spread. However, we cannot measure absolute delay as there is no synchronization. For each measurement instance, we conduct multiple Rx capture iterations (exceeding 10) and average the results to obtain one sample. Furthermore, three full repeats are acquired at each measurement distance point. During the pathloss measurements across various scenarios, we have excluded samples and distance points exhibiting a similar trend to prevent data redundancy on the graph. Also, we have expanded the number of sample points for distances where a sudden change is occurring.

C. MEASUREMENT SCENARIOS
The propagation measurement campaign at 28 GHz was performed in National Spectrum Centre, Frongoch farm
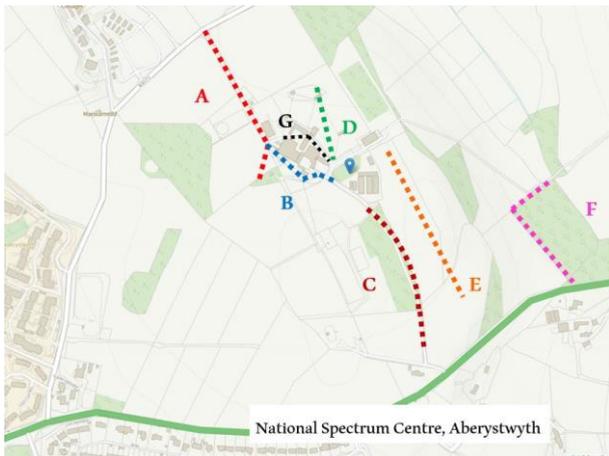

FIGURE 4. Map of the Frongoch farm with measurement routes

Aberystwyth, Wales, United Kingdom [42] (Lat.: 52.42384, Long: -4.05272). A map of the Frongoch farm and test routes is shown in Fig.4. Different environments in the Frongoch farm are considered for a detailed propagation study. In general, the routes consist of straight and curve roads, with various vegetations of bushes and woods. Propagation experiments were conducted in February 2023.

IV. PROPAGATION MEASUREMENTS
Measurements were conducted using two channel sounder modules, one as transmitter and other as receiver.

A. ROUTE A: STRAIGHT ROAD AND ELEVATED PATH
In the first measurement scenario A, we conducted two trials. Initial trial focused on the straight road (235 m) to analyze the propagation in a zero elevation situation. The Tx and Rx antennas were placed 1.2 m above ground. We have conducted measurements on 11 test locations with 3 localized tests per location. Fig. 5 shows the Route A and Route A_elevated. The Tx system was placed at the middle of the road with visibility down the road. The Rx system was
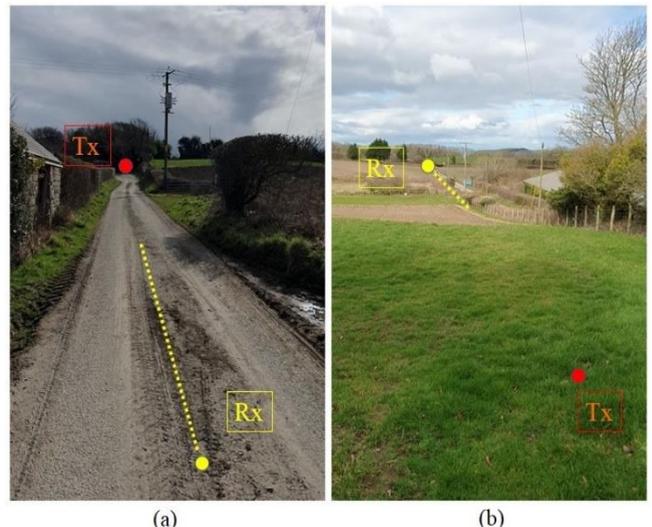

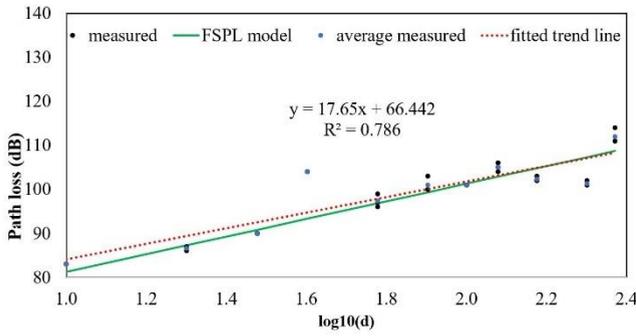**FIGURE 5. (a) Route A (b) Route A_elevated**

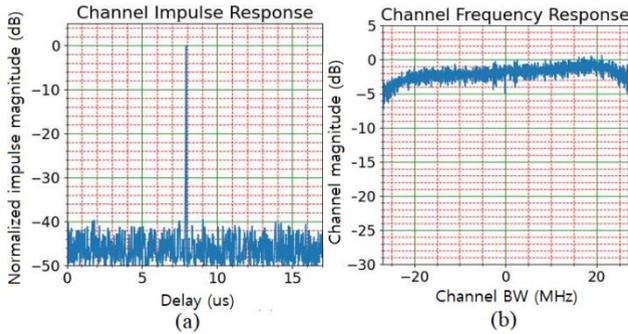**FIGURE 6. Extracted path loss of route A**

FIGURE 7. (a) Impulse response and (b) Channel frequency response in route A

moved along the road using a small hand trolley. Route A has a total distance of 235 m and A_elevated has 282 m LoS range. A_elevated route comprises of part of A route and small hill, approximately 10 m higher than road. In route A, the Tx was fixed at one end of the road and the Rx system was moved by trolley to each test location as in Fig. 5, whereas in A_elevated route the Tx was fixed at the top of the hill and Rx is moved along the straight road. From the received data, the path loss of route A is estimated as shown in Fig. 6 and it is similar to the FSPL.

$$PL_{(A)} = 17.65log_{10}(d) + 66.4 + X_{\sigma A} \quad (16)$$

It can be observed that by fitting the curve, an exponent of 17.65, which is close to the FSPL value of 20 is extracted. No reflections were observed throughout this route from inspecting the time domain impulse data. Fig. 7 shows the single impulse response and the flat channel frequency response measured in route A. Route A road has a small dip
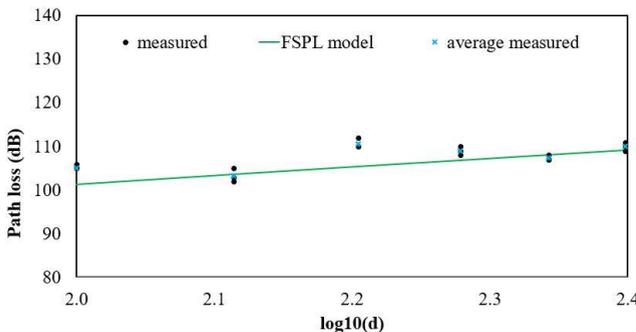

FIGURE 8. Extracted path loss of route A_elevated

near the Tx and then goes up again. Therefore, a variation in path loss can be seen around 50 m from the fitted curve and improvement in path loss as we reach the far end.

The calculated pathloss of route A_elevated obtained from measured data is shown in Fig. 8. To get the view of Tx, the measurements started at log(d) = 2 only. At initial test points, the measured path loss values are higher compared to FSPL due to the difference in Tx and Rx antenna heights. Tx and Rx alignment mismatch leads to the increased path loss in route, A_elevated. However, the angle between Tx and Rx decreases with increasing distance, making the path loss values similar to FSPL value. Due to the limited measurement points, it is difficult to depict the underlying trend with a curve.

B. ROUTE B: ZIG ZAG CURVED ROAD

Second scenario focused on zig zag road measurements. This experiment allows us to understand how the signal arrives in a curved road, where at some point the transmitter view is minimal by embankments and then improves. Finally, the complete view of the transmitter is blocked by vegetation and embankments as in Fig. 9(b). Antennas were placed at a height of 1.2m. Measurements were taken at 10 locations and 3 localized tests per location and has a total distance of 180 m. It can be observed from Fig. 9(a) that the intermediate receiving points Rx_1, Rx_2 and Rx_3 have distinct path loss pattern irrespective of the distance to the transmitter. Rx_1 has a direct LoS with the transmitter. But as the road curves, Rx_2 point has a narrow view of the transmitter, glances on an embankment by the road. Then, at Rx_3 point the receiver is able to find the transmitter view. As we go further down the road, the receiver lost the view of the transmitter completely.

Extracted path loss results from route B are shown in Fig. 10, compared to free space. It can be interesting to observe that the fitted curve is close to FSPL. From the measured results, the $\sigma B = 13.4\ dB$. $PL_{(offset)}$ is approximately 3 dB higher than the FSPL value. The fitted curve follows the free
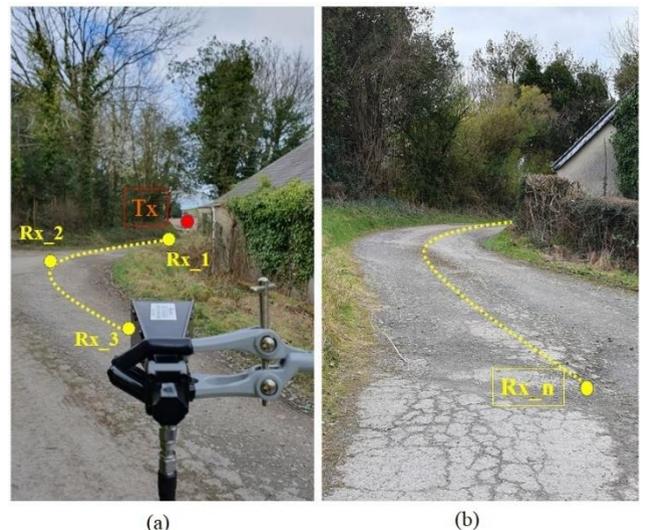

FIGURE 9. Route B (a) Different receiver positions with slight view of transmitter (b) Final receiver position no LoS
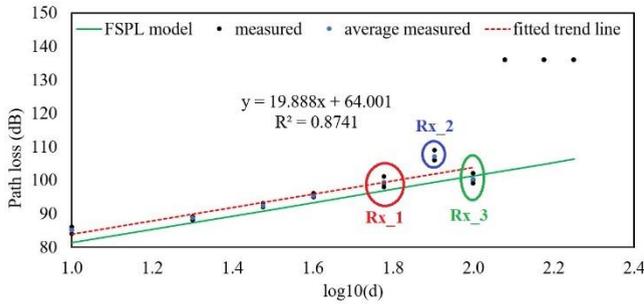
FIGURE 10. Extracted path loss of route B

space path loss with a very small offset. However, a sudden drop in pathloss can be observed at $\log10(d) = 1.9$. This is because of the narrow view of the transmitter due to the road embankments as in Rx_2 point of Fig. 7. Subsequently as the receiver reaches the Rx_3 point, a clear view of the transmitter is obtained. Therefore, at $\log10(d) = 2$ the path loss values are quite close to the free space values. Afterward, the receiver losses sight of the transmitter completely, and measured pathloss reaches measurement noise floor.

The exponent of the curve is 19.88 which is very close to the FSPL value. The pathloss has been fitted to the log-normal model as

$$PL_{(B)} = 19.88\log_{10}(d) + 64.01 + X_{\sigma B} \qquad (17)$$

It can be clearly observed that a narrow view of the Tx increases the path loss values and it increases beyond noise floor when the transmitter view is completely lost.

C. ROUTE C: C-SHAPED ROAD WITH TREES ON SIDES

In scenario C, a C shaped bend road with bushes and trees on either side of the road was used. The Tx horn was placed on the inside of bush and wooded bend, with gradually more woods obscuring path as in Fig. 11. This trial allows us to
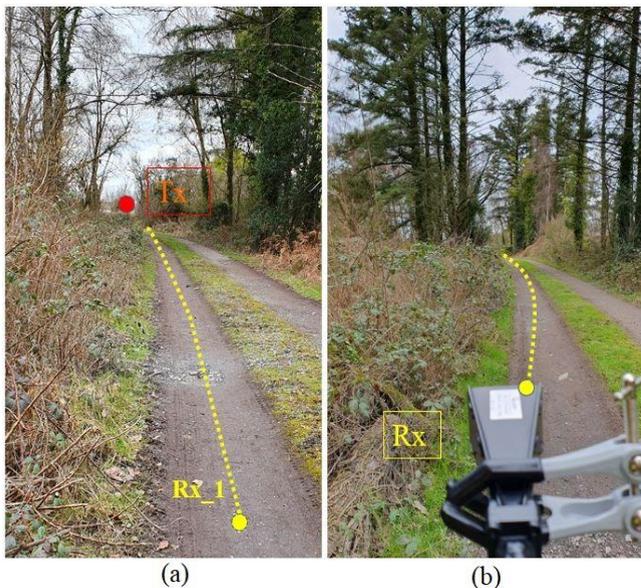

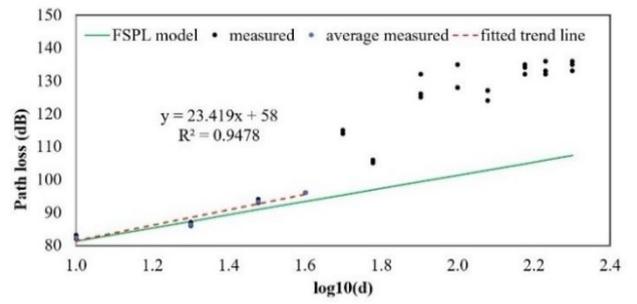**FIGURE 11.** Route C with different receiver positions (a)LOS view (b)NLOS view

FIGURE 12. Extracted path loss of route C with fitted curve till 50 m
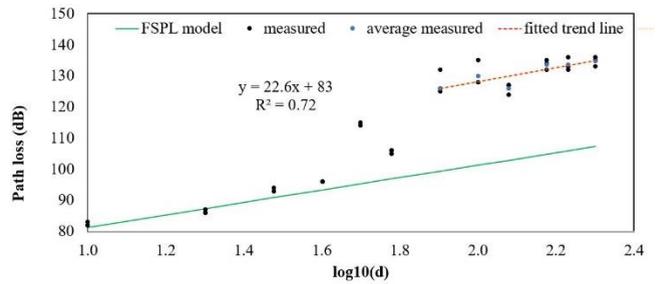

FIGURE 13. Extracted path loss of route C after 50 m

comprehend how the signal arrives in an environment where the receiver is surrounded by bushes and vegetation. Route C has a total distance of 250 m and measurements were carried out in 13 different test points again with 3 localized tests per location.

From the propagation measurements, the pathloss curve is plotted as shown in Fig.12 and Fig. 13. It can be observed that the pathloss can be analyzed with two models. In the first 50 m (Rx_1), the pathloss curve follows the free space values as in (18).

$$PL_{(C1)} = 23.42\log_{10}(d) + 58 + X_{\sigma C1} \qquad (18)$$

Within this range, the receiver maintains a direct line of sight to the transmitter, even though there is some obstruction from small bushes. However, beyond this point along the curved road, direct visibility of the transmitter is lost. The presence of vegetation and woods obstructs the transmitter's line of sight, resulting in a sudden and noticeable shift in the path loss values. During the initial measurements, the path loss closely resembles the FSPL up to 50m. The derived path loss exponent, n is 23.4, and the constant term $PL_{(offset)}$ is only 3 dB lower than FSPL.

$$PL_{(C2)} = 22.6\log_{10}(d) + 83 + X_{\sigma C2} \qquad (19)$$

After 50 m, the pathloss exponent changed to 22.6 dB which is similar to that in free space as shown in (19). However, the fixed term $PL_{(offset)}$ is 83 dB showing a significant offset from FSPL. This 22 dB increase in $PL_{(offset)}$ is due to the attenuation caused by the vegetation and woods. The excess path loss in this NLOS measurement is comparable to the NLOS excess pathloss due to foliage attenuation in [27].
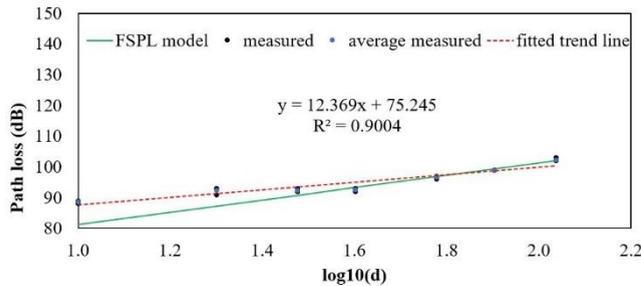
FIGURE 14. Route D tall grassland

FIGURE 15. Extracted path loss of route D

D. ROUTE D: TALL GRASSLANDS

To understand and study the effect of tall grasses in millimeter-wave propagation, a tall grassland is considered as route D as in Fig. 14. Route D has a distance of 109 m, and the grasses are nearly 1 m tall. In this experiment, the Tx and Rx antenna heights are reduced to 70 cm to make the propagation more through the grasses. From Fig. 14, it can be seen that the extracted path loss model is very close to FSPL values, suggesting any reflections are minimal. The path loss data has been fitted to the log-normal model (3), resulting in (21).

$$PL_{(D)} = 12.37 log_{10}(d) + 75.24 + X_{\sigma D} \qquad (20)$$

For the grassland measurement results σD = 2.4 dB. The fixed loss from a FSPL model at 1 m would be 61.4 dB. Thus, from (20) it can be seen that the fixed term $PL_{(offset)}$ is 14 dB higher than for FSPL. In (21) it can also be seen that the fitted path loss exponent n is 12.37, which is lower than expected for FSPL (in part due to the higher fixed loss term). The higher pathloss in the beginning may be due to pointing error or ground unevenness but it converges toward FSPL later as shown in Fig. 15. There are no significant resolvable reflections throughout the trial, as was confirmed by examining the time domain impulse data. At large distances, the measured path loss follows the FSPL, hence the measurement stopped at 109 m.

E. ROUTE E: HILL

For understanding the effect of a hill in close to ground millimeter-wave propagation, a hill with no tall grasses and trees are considered as route E as shown in Fig. 16. Route E

has a slant height of 210 m to the top of the hill, and it climbs down to a total distance of 250 m. In this experiment, the Tx and Rx antenna heights are 120 m from local ground, with the entire transmitter system also raised a further 70 cm on a platform. The receiver system is initially placed at the bottom of the small hill. From the propagation measurements, the pathloss is estimated and plotted as shown in Fig.17. It can be observed that the initial pathloss value is high due to the difference in antenna heights. Then the antenna beams are aligned, and it follows a FSPL curve as in Fig. 17 until 210 m. The path loss data has been fitted to the log-normal model as in (21)

$$PL_{(E)} = 25.43(d) + 55.92 + X_{\sigma E} \qquad (21)$$

For the hill measurement results σE = 8.3 dB. The fixed term $PL_{(offset)}$ is 5.4 dB lower than the FSPL. The path loss exponent n is 25.43, higher than the frees pace value and it is due to the difference in heights as it ascends the hill. Even though as the receiver system is moved towards the top of the hill and antenna heights change significantly, the pathloss curves are showing a fair similarity with free space values. It can be confirmed that a slight view of the transmitter is very much enough for the propagation and the beam widths of the antennas also helps. Around log(d) =2.3, it can be observed that the pathloss differs considerably with slight increase in distance. At this point, the receiver system reached the top of the hill and started to descend the hill. As it descends the receiver slowly loses the view of the transmitter antenna and the pathloss increases significantly. At 230 m from the transmitter, the receiver lost the complete view of transmitter. Thus, the measurement didn't continue further as it reached the noise floor.
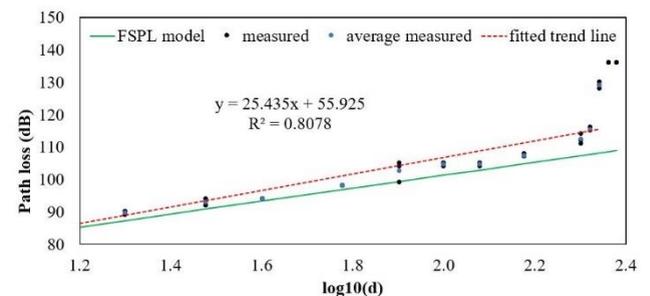

FIGURE 16. Route E hill

FIGURE 17. Extracted path loss of route E

F. ROUTE F: DENSE TREE FOREST

In scenario F, the measurements were carried out to analyze the pathloss in a dense tree forest as shown in Fig. 18. In this measurement, the propagation can be affected by the trees, from the penetration paths by leaves and reflections from the trees. In order to cover the maximum possible measurements in the available site through uniformly dense forest, both the transmitter and receiver units are moved. Initially, the Tx and Rx systems are placed 7 m apart and then increased gradually to 100 m where it reached the measurement noise floor. As the signal passed through dense forest from the initial measurement, the Tx and Rx alignment are roughly performed manually. The pathloss is estimated and plotted as shown in Fig. 19. It can be observed that this pathloss curve is different from the previous measurement significantly. From the initial point to final point, it follows a straight line, which is parallel to FSPL curve. So, it can be understood that a specific fixed attenuation is clearly caused due to the thick forest. An offset of nearly 32 dB can be observed directly from the Fig. 19 compared to free space path loss curve. As the distance increased from 10 to 100 m, the pathloss proportionally increased with distance. At 10 m, the measured pathloss shows an additional attenuation of around 30 dB compared to FSPL. Then around 100 m, the excess path loss due to dense tress increased to 35 dB. The path loss data has been fitted to the log-normal model as (22)

$$PL_{(F)} = 25.23(d) + 83.21 + X_{\sigma F} \qquad (22)$$

The pathloss exponent n is nearly 5 dB higher than the free space value of 20. The fixed term $PL_{(offset)}$ is 83.2 dB
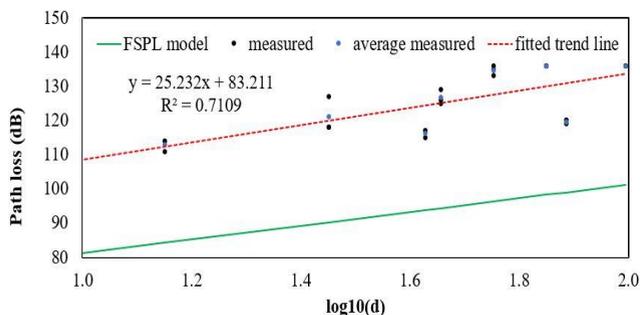
compared to 61 dB. From the measurements $\sigma F = 5.3$ dB. A foliage attenuation in the range of 15 to 40 dB is observed at 28 GHz in [22] in a similar distance range. However, that reported work conducted in a residential environment and not in a close to ground scenario.

G. ROUTE G: BUILDINGS

Finally, in order to analyze the reflection effects in a close to ground measurement the farmhouse area with buildings is considered as the last scenario. The total distance covered in this measurement is limited to nearly 100 m due to the scenario. In the initial 50 m, the Tx and Rx are in LoS with buildings on both sides as shown in Fig. 20. Then, the Rx antenna is moved further to 100 m but in these measurements the direct signal is almost lost due to the metal buildings in the farm. The measurements in this scenario started in the low gain mode of channel sounder. However as there is no LoS after 50m, the measured values are mainly due to reflection values only. Thus, the low gain mode of channel sounder gives very low values in the receiver side. Therefore, high gain mode of channel sounder is then utilized for measuring the signal and for estimating the pathloss. The extracted path loss results from this scenario are shown in Fig. 21, compared to free space values. It can be observed from Fig. 21 that for the initial 50 m, the measured pathloss values are closely to the free space values. The path loss data has been fitted to the log-normal model resulting in (23)

$$PL_{(G)} = 77.9(d) - 25.629 + X_{\sigma G} \qquad (23)$$

The path loss exponent n is estimated as 77.9, whereas the fixed term $PL_{(offset)}$= -25.69 dB. Reflections were observed in LoS range around the distances 20 and 40 m. These reflections are mainly caused by the sheet metal buildings.

FIGURE 18. Route F dense tree forest

FIGURE 19. Extracted path loss of route F

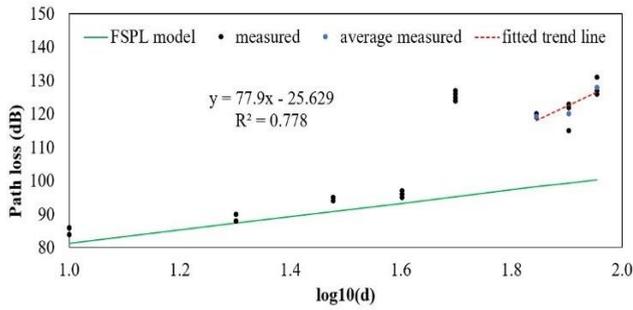FIGURE 20. Route G farmhouse buildings

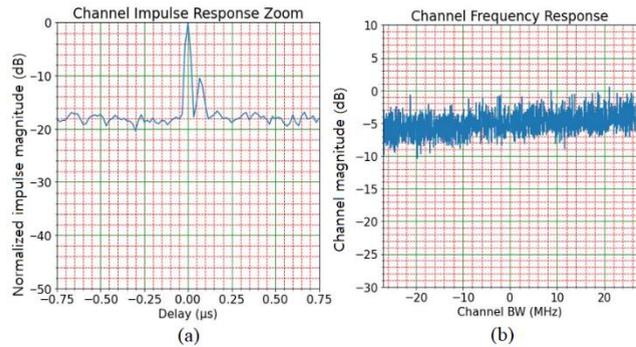**FIGURE 21.** Extracted path loss of route G

FIGURE 22. (a) Impulse response (b)Channel frequency response in route G at 20 m.

Impulse response and channel frequency response at 20 m are shown range are shown in Fig 22.

At 50 m, there is no LoS and only reflections can cause the received signal. It can be observed that at log(d) = 1.6, the measured pathloss is significantly reduced. Fig. 23 shows the impulse response and channel frequency response in route G at 80 m. As the Rx is moved further, strong reflections can be observed around log(d) = 1.9 as shown in Fig. 23, spreading across 75 ns. A path loss of around 120 dB at 50 m is measured from the multiple runs. At this stage, there is no LoS and pathloss is mainly dominated by the reflections from the building.

V. DISCUSSION AND ANALYSIS

The measurement results in diverse scenarios indicated that the path loss at millimeter-wave frequencies is heavily dependent on the terrains, buildings and vegetations on the path and vicinity of transmitter and receiver. To the best of our knowledge, this is the first work for close-to-ground propagation models at 28 GHz over different terrains and vegetation. Most of the existing millimeter-wave frequency propagation models are focused on short range indoor applications. Even though there are some outdoor works.

From the measurements, it can be estimate that routes with no obstructions achieved pathloss values similar to free space values. In straight and zig zag curved roads, the path loss exponent values are 17.65 and 19.88, i.e., in accordance with FSPL when there is LoS. However, in zig-zag curved
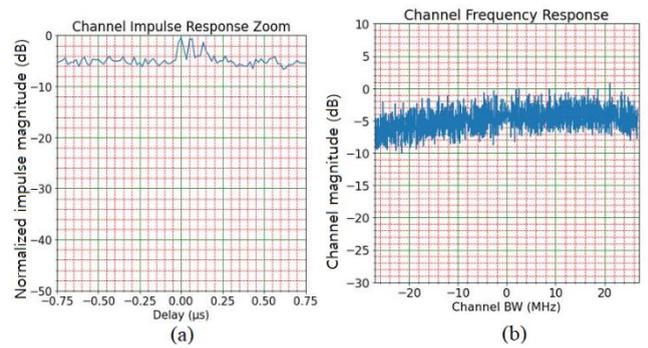

FIGURE 23. (a) Impulse response (b)Channel frequency response in route G at 80 m.

road the pathloss dropped and moves away from the fitted curve as in Fig. 9 due to road embankments at log(d)= 1.9. zag road. The fixed term $PL_{(offset)}$ is also estimated as 66.4 and 64 dB respectively in straight and zig-zag roads, which is close to the FSPL value.

In measurements with different Tx and Rx elevations, conducted in elevated path (Route A_elevated) and hill (Route E), the pathloss was visibly different compared to FSPL values. Even though the Tx had differing heights compared to Rx, the angle between Tx and Rx were decreasing with increasing distance. However, in hill measurements the Rx was gradually moved to the top of hill. So, the pathloss exponent was 5 dB higher than FSPL.

Important variations were observed in the measurements with vegetation. In the C shaped wood road (route C), after losing the direct view of Tx, the path losses were changed compared to the initial values with LoS. Values of n almost similar to FSPL and fixed offset increased by around 22 dB. But significant attenuation was not observed in tall grassland (route D) apart from slight variations in the initial values, possibly due to aiming difference or the short testable range. In dense tree measurements (route F) high attenuation was observed compared to FSPL and the attenuation was increased with distance as in Fig. 19. A very high offset of 83.2 dB was observed and also a high path loss exponent of 25.

To further analyze the measurement data conducted in dense trees, a comparison is presented with the foliage loss models as shown in Fig. 24. For plotting the pathloss against the distance, the foliage loss values have been added with the FSPL. It is clear that the measured path loss values are in the region of foliage loss model values. However, after 50 m the proposed measurement system receives better signal strength. The measured path loss values are lower than the previously discussed foliage loss models. At 28 GHz, ITU-R-235 model predicts slightly lower path loss values till 30 m, thereafter the model overestimates the path loss values. It can be observed that the FITU-R model overestimates the path loss. The COST235 model predicts very similar values in the initial measurements, however it slightly overpredicts around 100 m distance.

TABLE 1. Comparison of pathloss in different routes

Route	Description	Path loss exponent n	$PL_{(offset)}$	X_σ	Reflection
FSPL for 1m	Free space path loss for a reference distance of 1m	20	61.3	-	-
A	straight road &	17.65	66.4	3.9	No
B	zig zag curved road	19.88	64	13.4	No
C	c-shaped road with trees on sides	22.6	83	5.8	No
D	tall grasslands	12.37	75.24	2.4	No
E	Hill	25.43	55.9	8.3	No
F	dense tree forest	25.23	83.21	5.9	No
G	Buildings	77.9	-25.62	22.7	Strong reflections

A brief comparison of the propagation measurements with other similar works is presented in Table 2. In [24], near ground radio propagation at VHF and UHF bands is presented. A revision to the ITU-R model is suggested, incorporating the lateral wave effect. However, the measurement is in a tropical palm plantation with trees spaced around 7 m apart, it is hard to model a typical forest environment. Propagation through bushes and small tress were considered in [25] and [27] respectively at UHF bands. Similarly, propagation through coniferous and deciduous forest were investigated in [26],[28] and [29]. These reported close to ground propagation measurements were in VHF and UHF bands only.

Propagation at 28 GHz through vegetation in residential and urban area is analyzed in [21] and [22]. Hence, the building walls also contributed to the propagation paths and associated losses along with the tree cluster in the measurements. In [20], 24 GHz propagation through vegetation is investigated. Experiments suggested the need of revised ITU-R model. However, the transmitter is placed in tree level and receiver in close to ground level and the measurement considered only sub urban tree clutter scenario. These millimeter-wave propagation measurements in [20], [21] and [22] were focused on foliage attenuation.
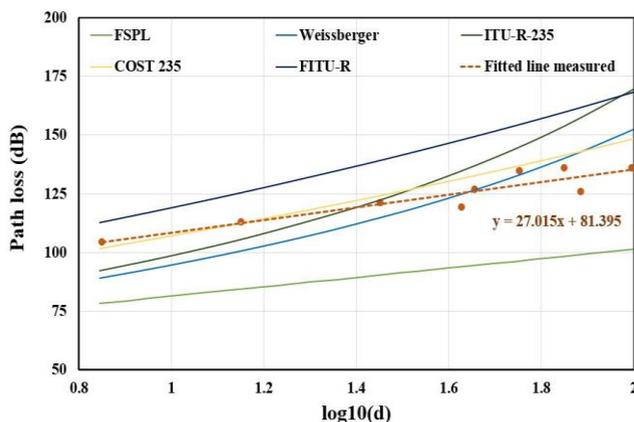
However, the transmitters in these works were placed in a higher height compared to receiver level. So, in author's knowledge, this proposed work is the first millimeter-wave close-to-ground propagation measured in rural outdoor scenarios. Then, the log-normal models derived from the measured propagation data are presented for diverse outdoor scenarios. Moreover, most of the other propagation works used expensive lab kits with trolleys [33],[34]. However, this proposed system is conveniently portable and made with commercially accessible integrated circuits (ICs) and generates graphs depicting channel frequency response and impulse delay spread measurements in the measurement site with no further delays for post processing.

VI. CONCLUSION

In this article, 28 GHz close-to-ground propagation measurements were performed with bespoke correlation based channel sounders for analyzing the channel models for different rural outdoor scenarios in the National Spectrum Centre, Aberystwyth. Large scale path loss, time domain impulses and channel responses of the diverse terrains were extracted from the measured data and log normal models were presented for all different terrains. Path losses similar to free space values were observed in straight road, zig-zag roads and in hill scenarios except in cases where the receiver lost the sight of the transmitter.

Propagation through forest has been analyzed with other foliage loss models. The proposed measurement system demonstrates enhanced signal strength when transmitting through dense trees and forest. The measurement data shows that the foliage loss models was overestimating the path loss values at 28 GHz. Strong reflections were observed in close to ground propagation through buildings at log(d) distance of 1.9, spreading across 75 ns. Path loss of 120 dB is estimated at this location with no LoS condition and thus, it is mainly dominated by the reflections from the building. The measured results and findings in this close to ground propagation research could be informative for forthcoming military and covert applications.

y = 27.015x + 81.395

FIGURE 24. Comparison of measured path loss with other foliage models.

IEEE Open Journal of
Antennas and Propagation

TABLE 2. Comparison with other similar foliage measurements.

Ref	Frequency (GHz)	Measurement scenarios	Tx heights (m)	Rx heights (m)	Range (m)	Measurement Equipment
[23]	0.3, 1.9	Deciduous forest	0.75 -1.55	0.75 -1.55	500	Software radio
[24]	0.24, 0.7	tropical plantation with average height of 5.6 m	2.15	2.15	1000	Lab kits
[25]	0.92, 2.4	Mulberry bushes	1.5	1.5	50	Lab kits
[26]	0.917	coniferous and deciduous forest	1.5-3.5	1.5-3.5	1000	Modules
[27]	3.5	Light trees and scrub land	2.1	2.1	40	Transmitter, receiver & power meter
[28]	0.9,1.8, 2.1	coniferous forest	2	2	400	Mobile phones
[29]	2.4	coniferous and deciduous forest	1.8	1.8	1028	Software radio
[21]	28	Vegetation in urban area	7	2	180	Lab kits
[22]	28	Vegetation in residential area	6	4	370	Lab kits
[20]	24	Suburban tree clutter	15	1.75	95	Lab kits
This work	**28**	**Straight roads** **Grasslands** **Hill** **Dense tree forest**	**1.2** **0.7** **1.2** **1.2**	**1.2** **0.7** **1.2** **1.2**	**235** **109** **230** **100**	**PCB module, SDR & Raspberry Pi**

REFERENCES

[1] Z. Pi and F. Khan, ''An introduction to millimeter-wave mobile broadband systems,'' *IEEE Commun. Mag.*, vol. 49, no. 6, pp. 101–107, Jun. 2011

[2] Y. Li, J. Yang, and N. Ansari, ''Cellular smartphone traffic and user behavior analysis,'' in *Proc. IEEE Int. Conf. Commun. (ICC)*, Jun. 2014, pp. 1326–1331.

[3] C. Casetti, "The challenges of universal broadband connectivity [Mobile Radio]," *IEEE Veh. Tech. Mag*, vol. 17, no. 3, pp. 5–11, Aug. 2022.

[4] S. Geng, J. Kivinen, X. Zhao, and P. Vainikainen, "Millimeter-wave propagation channel characterization for short-range wireless communications," *IEEE Trans. Veh. Technol.*, vol. 58, no. 1, pp. 3–13, Jan. 2009.

[5] X. Wu et al., "60-GHz millimeter-wave channel measurements and modeling for indoor office environments," *IEEE Trans. Antennas Propag.*, vol. 65, no. 4, pp. 1912–1924, Apr. 2017.

[6] Z. Hays, G. Richter, S. Berger, C. Baylis, and R. J. Marks, ''Alleviating airport WiFi congestion: A comparison of 2.4 GHz and 5 GHz WiFi usage and capabilities,'' in *Proc. Texas Symp. Wireless Microw. Circuits Syst. (WMCS)*, Apr. 2014, pp. 1–4. 3

[7] O. Kanhere and T. S. Rappaport, "Position location for futuristic cellular communications: 5G and beyond," *IEEE Commun. Mag.*, vol. 59, no. 1, pp. 70–75, Jan. 2021

[8] A. P. K. Reddy et al., "5G New Radio Key Performance Indicators Evaluation for IMT-2020 Radio Interface Technology," *IEEE Access*, vol. 9, pp. 112290-112311, 2021

[9] Q. C. Li et al., "5G Network Capacity: Key Elements and Technologies," *IEEE Vehic. Tech. Mag.*, vol. 9, no. 1, 2014, pp. 71–78.

[10] W. Roh et al., "Millimeter-wave beamforming as an enabling technology for 5G cellular communications: theoretical feasibility and prototype results, '' *IEEE Commun. Mag.*, vol. 52, no. 2, pp. 106-113, Feb. 2014.

[11] T. S. Rappaport et al., ''Millimeter-wave mobile communications for 5G cellular: It will work!'' *IEEE Access*, vol. 1, pp. 335–349, May 2013.

[12] T. S. Rappaport, R. W. Heath, Jr., R. C. Daniels, and J. N. Murdock, *Millimeter-wave Wireless Communications*, 1st ed. Upper Saddle River, NJ, USA: Prentice-Hall, 2015.

[13] J. Ko et al., "Feasibility study and spatial–temporal characteristics analysis for 28 GHz outdoor wireless channel modelling*," IET Commun.*, vol. 10, no. 17, pp. 2352–2362, Nov. 2016.

[14] J. Ko et al., "Millimeter-wave channel measurements and analysis for statistical spatial channel model in in-building and urban environments at 28 GHz," *IEEE Trans. Wireless Commun.*, vol. 16, no. 9, pp. 5853–5868, Sep. 2017.

[15] T. R. Fernandes, R. F. S. Caldeirinha, M. O. Al-nuaimi and J. Richter, "Radiative Energy Transfer Based Model for Radiowave Propagation in Inhomogeneous Forests," in *Proc. IEEE Veh. Techn. Conf.*, Canada, 2006.

[16] D. Didascalou, M. Younis, and W. Wiesbeck, "Millimeter-wave scattering and attenuation in limited vegetation structures," in *Proc. Int. Conf. Geosci. Remote Sens. Symp.*, Jul. 1999, pp. 1835–1838.

[17] F. Mani and C. Oestges, "A ray based method to evaluate scattering by vegetation elements," *IEEE Trans. Antennas Propag.*, vol. 60, no. 8, pp. 4006–4009, Aug. 2012.

[18] N. R. Leonor, R. F. S. Caldeirinha, T. R. Fernandes, D. Ferreira, and M. Sánchez, "A 2D ray-tracing based model for micro- and millimeterWave propagation through vegetation*," IEEE Trans. Antennas Propag.*, vol. 62, no. 12, pp. 6443–6453, Dec. 2014.

[19] F. Schwering, E. Violette, and R. Espeland, "Millimeter-wave propagation in vegetation: Experiments and theory," *IEEE Trans. Geosci. Remote Sens.*, vol. GRS-26, no. 3, pp. 355–367, May 1988.

[20] I. Rodriguez, R. Abreu, E. P. L. Almeida, M. Lauridsen, A. Loureiro, and P. Mogensen, "24 GHz cmwave radio propagation through vegetation: Suburban tree clutter attenuation," in *Proc. 10th Eur. Conf. Antennas Propag. (EuCAP)*, Apr. 2016, pp. 10–15.

[21] J. Ko *et al.*, "28 GHz millimeter-wave measurements and models for signal attenuation in vegetated areas," in *Proc. 11th Eur. Conf. Antennas Propag. (EUCAP)*, Mar. 2017, pp. 1808–1812.

[22] J. Ko *et al.*, "Measurements and analysis of radio propagation at 28 GHz in vegetated areas of typical residential environments," *IEEE

Trans. Antennas & Propag., vol. 68, no. 5, pp. 4149–4154, May 2020.

[23] G. G. Joshi *et al.*, ''Near-ground channel measurements over line-of-sight and forested paths,'' *IEEE Proc.-Microw., Antennas Propag.*, vol. 152, no. 6, pp. 589–596, Dec. 2005.

[24] Y. S. Meng, Y. H. Lee, and B. C. Ng, ''Empirical near ground path loss modeling in a forest at VHF and UHF Bands,'' *IEEE Trans. Antennas Propag.*, vol. 57, no. 5, pp. 1461–1468, May 2009.

[25] R. Yoshimura *et al.*, ''Effect of vegetation on radio wave propagation in 920-MHz and 2.4-GHz bands,'' in *Proc. Asia–Pacific Microw. Conf. (APMC)*, Dec. 2016, pp. 1–4.

[26] J. Hejselbæk, J. Ødum Nielsen, W. Fan and G. F. Pedersen, ''Empirical Study of Near Ground Propagation in Forest Terrain for Internet-of-Things Type Device-to-Device Communication, ,'' *IEEE Access*, vol. 6, pp. 54052-54063, 2018.

[27] M. Rodriguez, R. Feick, H. Carrasco, R. Valenzuela, M. Derpich, and L. Ahumada, ''Wireless access channels with near-ground level antennas,'' *IEEE Trans. Wireless Commun.*, vol. 11, no. 6, pp. 2204–2211, Jun. 2012.

[28] O. Kurnaz and S. Helhel, ''Near ground propagation model for pine tree forest environment,'' *Int. J. Electron. Commun.*, vol. 68, no. 10, pp. 944–950, Oct. 2014.

[29] D. P. Smith, G. G. Messier, and M. W. Wasson, ''Boreal Forest low antenna height propagation measurements,'' *IEEE Trans. Antennas Propag.*, vol. 64, no. 9, pp. 4004–4011, Sep. 2016.

[30] Y. Wang, Y. Lv, X. Yin, and J. Duan, "Measurement-based experimental statistical modelling of propagation channel in industrial IoT scenario," *Radio Science*, vol. 55, pp. 1-14, Sep. 2020.

[31] Y. Lyu, A. W. Mbugua, Z. Yuan, K. Olesen, and W. Fan, "Design and validation of a multilink phase-compensated long-range ultrawideband VNA-based channel sounder," *IEEE Trans. Microw. Theory & Tech.*, vol. 70, no. 10, pp. 4528-4543, Oct. 2022.

[32] B. B. Harianto, M. Hendrantoro, G. Ardiansyah, and A. Mauludiyanto, "Measurement of wideband indoor radio propagation channel using USRP," in *Proc J. of Physics: Conf. Series*, , vol. 1381, no. 1, pp. 1-10, Nov. 2019.

[33] J. Ko, S. U. Lee, Y. S. Kim, and D. J. Park, "Measurements and analyses of 28 GHz indoor channel propagation based on a synchronized channel sounder using directional antennas," *Journal of Electromag. Waves and App.*, vol. 30, no. 15, pp. 2039–2054, Oct. 2016.

[34] M. Samimi *et al.*, "28 GHz angle of arrival and angle of departure analysis for outdoor cellular communications using steerable beam antennas in New York City," in *Proc IEEE Vehic. Techn. Conference*, Dresden, 2013. pp. 1-6.

[35] H. Zhao *et al.*, "28 GHz millimeter-wave cellular communication measurements for reflection and penetration loss in and around buildings in New York city," in *Proc. IEEE Int. Conf. Commun.*, Budapest, 2013, pp. 5163–5167.

[36] J. Lee, J. Liang, J.-J. Park, and M.-D. Kim, "Beamwidth-dependent directional propagation loss analysis based on 28 and 38 GHz urban micro-cellular (UMi) measurements," in *Proc. 2017 IEEE 86th Vehi. Techn Conf. (VTC-Fall)*, Toronto, 2017, pp. 1–5.

[37] J. Du *et al.*, "Directional measurements in urban street canyons from macro rooftop sites at 28 GHz for 90 % outdoor coverage," *IEEE Trans. Antennas & Propag.*, vol. 69, no. 6, pp. 3459–3469, Jun. 2021.

[38] E. A. Ball and S. D. Joseph, "A Portable 28-GHz Channel Sounder Platform and Measurement Results from Close-to-Ground Field Tests," *IEEE Open J. Instrum. Meas.*, vol. 2, pp. 1-11, 2023.

[39] E. A. Ball, "Design and field trial measurement results for a portable and low-cost very-high-frequency / ultra-high-frequency channel sounder platform for Internet of things propagation research," *IET Microw*, vol. 13, no. 6, pp. 714–724, May 2019.

[40] H. T. Friis, ''A note on a simple transmission formula,'' in *Proc. IRE*, vol. 34, no. 5, pp. 254–256, May 1946.

[41] J. D. Parsons, *The Mobile Radio Propagation Channel*. Hoboken, NJ, USA: Wiley, 2000.

[42] National Spectrum Centre Aberystwyth University website. [Online]. Available : https://www.spectrum.aber.ac.uk/

[43] A. H. Lagrone, ''Forecasting television service fields,'' in *Proc. IRE*, vol. 48, no. 6, pp. 1009–1015, Jun. 1960.

[44] M. A. Weissberger, ''An initial critical summary of models for predicting the attenuation of radio waves by trees,'' Tech. Rep., 1982.

[45] ''Influences of terrain irregularities and vegetation on tropospheric propagation,'' CCIR, Geneva, Switzerland, Tech. Rep. 235-6, 1986.

[46] *European Commission; Directorate-General for Telecommunications, Information Market and Exploitation of Research, COST 235: Radiowave Propagation Effects on Next-Generation Fixed-Services Terrestrial Telecommunications Systems*, OPOCE, 1996.

[47] M. O. Al-Nuaimi and R. B. L. Stephens, ''Measurements and prediction model optimisation for signal attenuation in vegetation media at centimetre wave frequencies,'' *IEE Proc. Microw., Antennas Propag.*, vol. 145, no. 3, pp. 201–206, Jun. 1998.

SUMIN DAVID JOSEPH (Member, IEEE) received the B.Tech. degree (Hons.) in electronics and communication from the CUSAT University, India, in 2012, M. Tech. degree (Hons.) in communication systems from the Visvesvaraya National Institute of Technology, India, in 2015, and dual PhD degree (distinction) in electrical engineering from the University of Liverpool, U.K., and National Tsing Hua University, Taiwan in 2021.

Dr Sumin is currently working as a Post-Doctoral Research Associate with The University of Sheffield. He was a Lab Engineer under CoE with the Visvesvaraya National Institute of Technology, India from 2015 to 2017, where he was involved in projects of national importance.

Dr Sumin has authored or coauthored more than 30 articles in peer-reviewed journals and conference proceedings. His research interests include self-biased circulators, mm-wave antenna arrays, rectifying antennas, MMIC circuits, RFIC, rectifiers, integrated circuit designs, flexible electronics, wireless power transfer, energy harvesting and TMA antenna arrays. Dr Sumin is a technical reviewer for leading academic journals and conferences, including IEEE Transactions of Antenna and Propagation, IEEE Antenna and Wireless Propagation Letters and IEEE Access.

BILL GAVIN received his 1st Class MEng from The University of Sheffield in 2020. H is now working towards his PhD covering machine learning applied to the physical layer of communications systems at The University of Sheffield since October 2021. His research interests are the application of machine learning algorithms to communication systems and the hardware acceleration for artificial intelligence.

EDWARD A. BALL (Member, IEEE) was born in Blackpool, U.K., in November 1973. He received the Master of Engineering degree (Hons.) in electronic systems engineering from the University of York, York, U.K., in 1996.

After graduating, he worked in industry for 20 years, first spending 15 years working as an Engineer, a Senior RF Engineer, and finally the Principal RF Engineer at Cambridge Consultants Ltd., Cambridge, U.K. He then spent five years as the Principal RF Engineer and a Radio Systems Architect at Tunstall Healthcare Ltd., Whitley, U.K. In November 2015, he joined the Department of Electronic and Electrical Engineering, The University of Sheffield, Sheffield, U.K., where he is currently working as a Reader in RF Engineering and has a UKRI Future Leaders Fellowship. His research interests cover all areas of radio technology, from RF system design, RF circuit design (sub-GHz to mm-wave), and the application of radio technology to real-world industrial and commercial problems. He has a particular passion for RF hardware design. Mr. Ball is a member of the IEEE, IET and is a Chartered Engineer.